Published in final edited form as:
Dev Cell. 2012 March 13; 22(3): 530–543. doi:10.1016/j.devcel.2011.12.026.

ADF/Cofilin regulates actomyosin assembly through competitive inhibition of myosin II binding to F-actin

O'Neil Wiggan[1], **Alisa E. Shaw**[1], **Jennifer G. DeLuca**[1,2], and **James R. Bamburg**[1,2]

[1]Department of Biochemistry and Molecular Biology, Colorado State University, Fort Collins, CO 80523, USA

Summary

The contractile actin cortex is important for diverse fundamental cell processes, however, little is known about how the assembly of F-actin and myosin II motors is regulated. We report that depletion of ADF/cofilin proteins in human cells causes increased contractile cortical actomyosin assembly. Remarkably, our data reveal that the major cellular defects resulting from ADF/cofilin depletion, including cortical F-actin accumulation, were largely due to excessive myosin II activity. We identify that ADF/cofilins from unicellular organisms to humans share a conserved activity to inhibit myosin II binding to F-actin, indicating a mechanistic rationale for our cellular results. Our study establishes an essential requirement for ADF/cofilin proteins in the control of normal cortical contractility and in processes such as mitotic karyokinesis. We propose that ADF/cofilin proteins are necessary for controlling actomyosin assembly and intracellular contractile force generation, a function of equal physiological importance to their established roles in mediating F-actin turnover.

Introduction

Dynamic F-actin remodeling and the generation of cortical contractile forces are critical for cell morphogenesis, cell migration, cell division and other fundamental cellular functions (Bray and White, 1988; Clark et al., 2007). Assemblies of F-actin and myosin II motors generate cortical forces that influence hydrodynamic properties of the cytosol, dictate cell shape, control stem cell differentiation, and drive plasma membrane protrusions utilized in processes varying from cell motility to viral infection (Paluch et al., 2006; Clark et al., 2007). Our understanding of how the organization of cortical actomyosin is regulated is critical for many aspects of cell biology.

Proper spatial and temporal control of the actomyosin contractile apparatus must be maintained for normal cell function. For example, certain modes of polarized cell migration utilize concentrated actomyosin contractile forces at the rear of the cell while restricting these forces at the leading edge. Further, excessive cortical contractile forces may drive increased intracellular hydrostatic pressure and cortical instability resulting in features such as membrane blebbing (Charras and Paluch, 2008). The assembly of myosin bipolar

Corresponding Author: O'Neil Wiggan, Department of Biochemistry and Molecular Biology, Colorado State University, Fort Collins, CO 80523-1870, Phone: (970) 491-0208, FAX: (970) 491-0494, owiggan@colostate.edu.
[2]Equal contributing senior authors

filaments and motor activity are regulated by multiple mechanisms, for instance, by phosphorylation of the regulatory light chain by kinases such as myosin light chain kinase (Vicente-Manzanares et al., 2009). The manner in which the association of myosin motors with F-actin is regulated in a dynamic spatio-temporal manner remains an essential area of elucidation, as recently reviewed (Lecuit et al., 2010).

Actin depolymerizing factor (ADF)/cofilin-family proteins are important regulators of actin dynamics and are required for viability in organisms ranging from yeast to mammals (Pollard and Borisy, 2003; DesMarais et al., 2005; Bamburg and Bernstein, 2010). The activities of ADF/cofilin and their regulation are complex and current models indicate roles for them primarily in promoting F-actin turnover through severing and/or depolymerization. (Van Troys et al., 2008). Their actin dynamizing activity is inhibited through multiple mechanisms, a subset of which include; phosphorylation at a conserved Ser3 residue by kinases such as LIM kinase (LIMK), binding to phosphoinositides, and through competition for F-actin binding with certain tropomyosins (reviewed in Van Troys et al., 2008).

Here we examine the role of ADF/cofilin in patterning of the cortical actomyosin cytoskeleton. We identify that a significant role for ADF/cofilin in cells is to regulate myosin II function. Our results indicate an essential role for ADF/cofilin in modulating intracellular contractile forces and in maintenance of normal integrity of the cortical actomyosin cytoskeleton.

Results

Cofilin silencing induces plasma membrane blebbing and aberrant cortical F-actin organization

HeLa cells express both ADF and cofilin, however as is generally the case in most mammalian tissues, cofilin expression is predominant (Fig. 1C). To evaluate the requirements for ADF/cofilin in organization of the cortical actin cytoskeleton their expression was silenced using siRNA oligonucleotides. Cofilin protein levels were reduced on average by 75% and total ADF/cofilin levels by 96% at 72h following transfection of siRNAs targeted specifically to either cofilin, or cofilin and ADF respectively. Similar results were obtained using at least two different siRNA sequences for both ADF and cofilin (Fig. S1A). Live cell differential interference contrast (DIC) imaging revealed that greater than 80% of cells treated with siRNAs for cofilin or both cofilin and ADF (COF+ADF) displayed extensive plasma membrane blebbing compared to averages of 4% and 2% in ADF or control siRNA treated cells (Fig. 1A, B). Cell blebbing persisted over long periods beginning as early as 30h post cofilin siRNA transfection and became more abundant over 72h, correlating with the time course of cofilin depletion. This observation demonstrated that blebs induced following cofilin silencing were not due to apoptosis. Consistent with this conclusion we did not observe fragmented nuclei in fixed cells with blebs following cofilin silencing (data not shown). Blebbing in cofilin depleted cells was associated with strong accumulation of cortical circumferential F-actin bundles (basal and mid planes, Fig. 1D). F-actin organization was even more perturbed following COF+ADF depletion. These cells also had increased cortical F-actin bundles (Fig. 1D), and displayed intense abnormal F-actin accumulation at the base of large membrane bleb protrusions (Fig. 1E, right panels) and at the base of rosettes of smaller apical membrane blebs (Fig. 1E, left panels). The overall F-actin organization in ADF depleted cells was not significantly different from control cells. The severe F-actin abnormalities in COF+ADF depleted cells relative to cells in which only a single isoform was depleted, however, suggests that total ADF/cofilin activity is important for normal cytoarchitecture.

Depletion of both ADF and cofilin results in persistent blebs and abnormal contractile F-actin structures

Live cell 4D time-lapse imaging of cells expressing GFP-actin and depleted of both ADF and cofilin exposed significant differences in membrane and cortical F-actin dynamics in comparison to cells depleted of cofilin alone (Fig. 2). Blebs in cofilin-depleted cells were dynamic and displayed a life cycle similar to that previously reported for blebs induced by other conditions (Charras and Paluch, 2008). Blebs most commonly emerged from ruptures in the cortical actin cytoskeleton and were devoid of a detectable submembranous actin cortex up to the point of maximal expansion (Fig 2A). Bleb retraction correlated with formation of a new actin cortex at blebs (Fig. 2A, t = 31s). These features are readily evident in kymographs of a bleb life cycle (Fig. 2C). Blebs in cofilin depleted cells were relatively short lived (mean 73s) from the time of first appearance to complete retraction. In COF +ADF depleted cells actin accumulated in numerous puncta (Fig. 2E). These abnormal actin structures were not randomly distributed but instead were localized precisely to the base of membrane blebs (see overlays Fig. 2E), as seen earlier in fixed cells (Fig. 1E). Abnormal actin aggregates formed at the base of blebs only after bleb expansion (Fig. 2E, arrow; Fig. 2B and Movie S1) and resulted from constriction of an actin contractile ring structure (Fig. 2F) which contracted at a mean rate of 0.045 μm/s ± 0.009 (n = 13). Accumulation of a contractile actin structure at the base of blebs correlated with altered bleb dynamics, and 100% of blebs (n >300) with such structures failed to complete bleb retraction within 4 min. Blebs that accumulated actin at their base in COF+ADF depleted cells persisted for periods of over 20 min, significantly longer than the mean life time of 73s for blebs obtained following depletion of cofilin alone. On average, 87% of COF+ADF depleted cells had blebs with a persistent phenotype, in contrast to less than 1% of cells where only cofilin was depleted (Fig. 2G). Rosette-like clustering of persistent blebs in COF+ADF depleted cells (Fig. 1E) was in part due to retrograde transport of blebs (mean velocity 0.007 μm/s; Fig. 2H, kymograph), via the contractile actin foci at the base of blebs which tethered blebs to underlying actin filaments (Fig. 2E, insets).

Persistent blebs in COF+ADF depleted cells failed to reassemble a new F-actin cortex (Fig. 2B, D), in comparison to dynamic blebs in cofilin depleted cells where a new cortex formed within seconds after expansion (Fig. 2A, C). Live imaging of COF+ADF depleted cells expressing either GFP-myosin IIA (Fig. 2I) or GFP-myosin IIB (Fig. 2J) revealed accumulation of these proteins in contractile structures at the base of blebs which became persistent, confirming the actomyosin composition of these aberrant structures.

We determined whether inactivation of cofilin through phospho-regulation could induce similar effects to those observed by silencing cofilin. Expression of either LIMK1 (not shown) or LIMK2 (Fig. S2) resulted in similar phenotypes to those obtained in COF+ADF depleted cells. LIMK2 expression induced the formation of both dynamic and persistent blebs, the latter of which accumulated contractile actin structures at their base (Fig. S2A). These defects were dependent upon intact kinase activity and were rescued by either co-expression of a Xenopus ADF/cofilin mutant which could not be phosphorylated (XAC-A3) or by co-expression of the cofilin activating phosphatase slingshot-1L (Fig. S2B). ADF/cofilin proteins, therefore, appear to be the primary LIMK regulatory target that mediates the abnormal membrane and contractile actin structures following LIMK overexpression.

ADF/Cofilin depletion results in increased cortical actomyosin assembly and increased filament contractility

Bleb induction, formation of ectopic contractile actin structures and failure of blebs to assemble a new contractile actomyosin cortex in ADF/cofilin depleted cells all suggested possible deregulation of actomyosin contractile assemblies following silencing of ADF and

cofilin. Blebbing, for example, in cofilin depleted cells may be the result of increased cortical tension and resultant greater cytosolic hydrostatic pressure (Tinevez et al., 2009). We examined the expression and distribution of endogenous myosin II motors, which are genetically encoded by one of three myosin heavy chain isoforms, myosin IIA (myoIIA), myosin IIB (myoIIB), or myosin IIC (myoIIC) (Vicente-Manzanares et al., 2009). HeLa cells used for this study expressed myoIIA and myoIIB but not myoIIC (Fig. 3; Fig. S1B, C and data not shown). Immunostaining for myoIIA and myoIIB revealed punctate staining, with accumulation of myosin along stress fibers and at the cell cortex (Fig. 3A, B). Cofilin silencing resulted in a strong increase in cortical myosin II accumulation (Fig. 3A), corresponding with the increased cortical F-actin bundles seen in these cells (Fig. 1D). Myosin puncta along actin filaments gave rise to discrete intensity peaks in fluorescence linescans (Fig. 3C, top). Along actin filaments, myosin intensity was greater and myosin puncta more densely packed (broader and more condensed peaks) in cofilin-depleted cells, relative to ADF-depleted cells or controls (Fig. 3B, C). Increased actomyosin assembly following ADF/cofilin depletion did not appear to involve elevation of total myosin II protein levels (Fig. S1D). Myosin activity was evaluated through immunostaining with antibodies to phospho-myosin light chain (Fig. 3A, D; p-MLC). At the cell cortex, p-MLC levels increased 1.7-fold for ADF depleted cells ($p < 0.0001$), and 4-fold for cofilin depleted cells ($p < 0.0001$), relative to control (Fig. 3A, D).

In cultured cells actin stress fibers are maintained under isometric tension (prestress) and normally display little contractile activity. Treatment of cells with drugs that destabilize the actin cytoskeleton network induces fiber contraction, explained by a solation-contraction coupling model (Kolega et al., 1991). In cells expressing RFP-Lifeact, for F-actin labeling, contraction of stress fibers was observed within 3 minutes following latrunculin B (sequesters G-actin) treatment. Contraction of fibers frequently resulted in fissure of cortical fibers as illustrated in Fig. 3E. Decreased actin intensity and fiber thinning at sites of fiber fissure accompanied by increased actin intensity adjacent to these sites, prior to breakage, was evidence of fiber strain and consistent with fissure due to tensile forces resulting from fiber contractility. Upon breakage, stress fibers display immediate ($\leq$ 30s) recoil retraction kinetics with viscoelastic properties (Kumar et al., 2006). In accordance with Hooke's law, the initial recoil kinetics of fibers will be proportional to the tension experienced by these fibers prior to separation. Upon fissure, the initial fiber retraction distance was on average 2.8-fold greater in cofilin depleted cells relative to control cells ($p = 0.003$, Fig. 3G). Furthermore, cofilin depleted cells achieved greater total retraction distances and retracted at faster rates (Fig. 3G).

In agreement with previous reports (Kolega et al., 1991; Kumar et al., 2006), it was evident from our images that fiber retraction after fissure was not due simply to depolymerization of filament ends, even on a time scale of over 3 minutes. For example, broken fibers with branches retracted while maintaining branched ends (Fig. S3) and fiber fragments displayed immediate retraction kinetics in accordance with apparent biases to the contractile forces present prior to breakage (compare higher actin intensity on left side of fissure point, Fig. 3E to faster immediate retraction kinetics Fig. 3F). Interestingly, the retraction kinetics of fibers at fissure sites from both control and cofilin depleted cells fit well to the Kelvin-Voigt model of a viscoelastic material, though with different curve features for each treatment (Fig. 3H). The mean visocoelastic time constant, τ, a ratio of viscosity to the elastic modulus, was greater in control cells (306 ± 228 s) relative to cofilin depleted cells (142 ± 112 s) consistent with greater fiber tension in cofilin depleted cells. Together, these data support the conclusion that cofilin depletion results in elevated actomyosin contractility and increased cytoskeletal prestress.

Rescue of cytoskeletal defects in ADF/cofilin depleted cells by myosin II silencing

We confirmed that excessive actomyosin assembly and membrane defects that arose following ADF/cofilin siRNA silencing were specifically due to the loss of ADF/cofilin activity through silence and rescue experiments. Expression of wild type XAC, which is not targeted by the ADF/cofilin siRNAs, or expression of a human cofilin made refractory to the cofilin siRNA (hCOF siRes), resulted in efficient rescue of all bleb phenotypes following COF+ADF siRNA treatments (Fig. 4A, B). Rescue was dependent upon the ability of the heterologous cofilins to efficiently bind actin since constitutively inactive phosphomimetics (E3) failed to rescue, in contrast to wild type or constitutively active (A3) proteins (Fig. 4B).

Next, we evaluated the specific requirements for myoIIA and IIB in defects which occur following ADF/cofilin depletion by siRNA co-silencing of each respective myosin. Using two distinct siRNAs for each myosin, western blot analysis revealed efficient silencing of each myosin (Fig. S1B, C), however, silencing of each myosin also affected expression of the other non-targeted myosin, regardless of the siRNA sequence used. Lower expression of non-targeted myosin IIB appeared to be due to proteolysis (Fig. S1C) and suggests that loss of cellular actomyosin structures may induce myosin II instability. Nevertheless, silencing of each individual myosin alone resulted in distinct cellular phenotypes (Fig. 4C–F), consistent with previous reports (Vicente-Manzanares et al., 2007). MyoIIA silencing gave rise to increased numbers of cells with an elongated phenotype and long tails (Fig. 4C), and to cells with a greater length to width ratio relative to myoIIB silenced cells or controls (Fig. 4D). MyoIIB silenced cells in contrast were more spread, as evident by an increase in cell area in these cells relative to myoIIA silenced cells or controls (Fig. 4E). Silencing of either myosin caused a reduction in stress fiber assembly (Fig. 4C). Significantly, silencing of either myoIIA or IIB in COF+ADF depleted cells efficiently blocked all bleb phenotypes and aberrant actomyosin assemblies (Fig. 4C, F). Instead of blebs, COF+ADF depleted cells in which either myoIIA or IIB were silenced produced numerous F-actin rich filopodial membrane protrusions (Fig. 4C). These results confirm an essential role for myosin II function in driving the bleb and cortical cytoskeletal defects that occur following ADF/cofilin depletion.

Myosin II activity controls bleb dynamics and aberrant cortical actin assembly in ADF/cofilin depleted cells

To further assess how myosin II activity contributes to the membrane and cytoskeletal defects following ADF/cofilin depletion, we treated live cells with blebbistatin, a drug which inhibits the ATPase cycle of type II myosins and sequesters them in a weak F-actin binding state (Straight et al., 2003; Kovacs et al., 2004). Blebbistatin treatment efficiently inhibited dynamic blebbing in cells depleted of cofilin alone or both cofilin and ADF (Fig. 5A–C; Movie S2). Remarkably, blebbistatin treatment also caused retraction of persistent blebs and disassembly of abnormal cortical actomyosin structures in COF+ADF depleted cells (Fig. 5B, D–F; Movie S3). Persistent blebs which had not developed a new actin cortex for over 10 minutes prior to blebbistatin treatment did so simultaneous to dissolution of actin aggregates at the base of blebs, following drug treatment (Fig. 5F, Movie S3). From these results we conclude that abnormal cortical F-actin accumulation in ADF/cofilin-depleted cells results primarily from excessive myosin II activity. Furthermore, it is this excessive myosin activity that drives all the features of elevated actomyosin contractility resulting in both dynamic and persistent bleb formation following ADF/cofilin depletion.

Competitive inhibition of myosin S1 binding to F-actin by ADF/cofilin

Increased actomyosin contractility and cortical tension following cofilin depletion are unlikely to result merely from actin filament stabilization since filaments by themselves are not contractile. Previous studies suggested that cofilin alters the actin-activated ATPase

activity of myosin II (Nishida et al., 1984; Abe and Obinata, 1989), however the precise mechanism by which cofilin may regulate myosin II activity is unknown. Structural and biochemical studies suggest that the primary binding site of actin for ADF/cofilin-family proteins and myosin II significantly overlap (Fig. 6A, B; McGough, 1998; Mannherz et al., 2007; Paavilainen et al., 2008; Lorenz and Holmes, 2010). Both protein families are suggested to make similar contacts with two adjacent actin subunits along the longitudinal axis of F-actin. We therefore hypothesized that ADF/cofilin may regulate actomyosin assembly through direct competition for F-actin binding with myosin II motors. To assess competition, the S1 subfragment of skeletal myosin II, which contains all the F-actin binding and motor activity of full myosin II, was utilized in F-actin cosedimentation assays along with recombinant ADF/cofilins (Fig. 6C–F). Cofilin at concentrations ~ 10-fold in excess of myosin S1 efficiently inhibited myosin S1 binding to F-actin and weak competition was observed even when both proteins were at approximately equivalent molar ratios. Inhibition occurred regardless whether myosin was preincubated with F-actin prior to cofilin addition (Fig. 6C), both proteins exposed to F-actin simultaneously (Fig. 6D–F), in the presence of low levels of ATP (120 μM, Fig. 6D–F); or in the absence of ATP, where the affinity of myosin for F-actin is greatest (Fig. 6D).

Binding of myosin S1 to F-actin was inhibited by ADF/cofilins from diverse organisms, albeit with different efficiencies (Fig. 6E–F). F-actin depolymerization was variable amongst the different ADF/cofilins, for example, minimal with Xenopus XAC and higher with chick ADF (compare actin in supernatants, Fig. 6C, E). Nonetheless, F-actin depolymerization was not a significant contributing factor to the reduced levels of myosin S1 co-pelleting with F-actin in the presence of ADF/cofilins as indicated by decreased molar ratios of myosin S1 to actin in pellets under each condition (Fig. 6F). Inhibition of myosin binding to F-actin by ADF/cofilin, however, appears dependent on efficient F-actin binding by ADF/cofilin since a phosphomimetic mutant which is impaired at F-actin binding failed to inhibit myosin S1 binding to F-actin (chick ADF E3, Fig. 6E–F). All together, these data support the conclusion that ADF/cofilins from diverse organisms share a conserved activity for competitive inhibition of myosin II binding to F-actin.

ADF/Cofilin is required for normal karyokinesis

A recent report suggested that aberrant actomyosin contractility and plasma membrane blebbing at the onset of cytokinesis contributes to spindle positioning defects (Rankin and Wordeman, 2010). We therefore investigated whether depletion of ADF or cofilin affected chromosome segregation (karyokinesis) during mitotic cell division. Analyses of fixed cells revealed a marked increase in cells with impaired chromosome segregation following silencing of either ADF or cofilin, relative to controls (Fig. 7C). Failed chromosome segregation resulted in daughter cells at telophase (Fig. 7A) and late cytokinesis (Fig. 7B) which were devoid of any DNA. Most cofilin depleted cells with abnormal karyokinesis also exhibited a distinct cytokinesis defect exemplified by the maintenance of a midbody between daughter cells at the final steps of cytokinesis (Fig. 7B, inset). Thus, our results identify a role for ADF/cofilin in regulating normal karyokinesis and are also consistent with previous reports which distinctly demonstrated roles for ADF/cofilin in cytokinesis (Gunsalus et al., 1995; Hotulainen et al., 2005).

We utilized live cell time-lapse imaging as a tool to better understand the cellular mechanisms which contributed to the karyokinesis defects in ADF or cofilin depleted cells and the relationship of plasma membrane blebbing to this process. All HeLa cells, regardless of siRNA treatment, exhibited dynamic plasma membrane blebbing with the onset of cytokinesis (Fig. 7D, F; Movie S4). Cells depleted of ADF or cofilin also produced dynamic blebs during metaphase, a behavior not observed in control cells (Fig. 7E, F). Additionally, during cytokinesis ADF/cofilin depleted cells also displayed behavior which resulted in

cycles of back and forth chromosome displacement (spindle oscillation, Fig. 7F, G–H). Few control cells showed this spindle oscillation behavior (~8%, Fig. 7F); and these cells displayed only small chromosome displacements, such that chromosomes never passed through the cleavage furrow site. Greater numbers of ADF depleted (36%) and cofilin depleted (63%) cytokinetic cells displayed spindle oscillation behavior. Furthermore, chromosome displacement in some ADF or cofilin depleted cells was large enough to allow repeated passage of chromosomes through the cleavage furrow from one daughter cell to another (Fig. 7H; Movie S5). This dynamic displacement of chromosomes occurred concomitant with cortical contraction of one daughter cell and cortical expansion, as result of cytoplasmic flow, to the opposing cell. Measurements of bleb height and diameter (Fig. 7I) during cytokinesis showed an increase in the size of both bleb parameters in ADF or cofilin depleted cells, relative to controls (Fig. 7J). Conspicuously, the population of control cells which displayed spindle oscillation behavior had a similar bleb height/diameter size distribution to ADF or cofilin depleted cells in contrast to control cells that did not undergo spindle oscillation (Fig. 7K, L). Inspection of control cells which underwent spindle oscillation (5/65 cells) revealed that these cells all produced a bleb which was greater than 10 μm in diameter (Fig. 7L). Significantly, chromosome displacement invariably correlated with retraction of a large diameter bleb (for example see Fig. 7G, arrowhead). At cytokinesis, the contractile forces exerted during retraction of the larger blebs produced by cells deficient for either ADF or cofilin are therefore likely the motive factor of increased spindle oscillation. Taken together, the results here are consistent with a key requirement for ADF/cofilin in the regulation of cortical contractile forces and tension during mitotic cell division.

Discussion

Our results reveal that a significant but hitherto unappreciated cellular role for ADF/cofilin-family proteins is that of myosin II regulation. Depletion of cofilin in human HeLa cells caused increased cortical actomyosin II assembly, accompanied by increased cortical contractility and tension, culminating in membrane blebs. Non apoptotic membrane blebs are proposed to be a cell tension release mechanism (Sedzinski et al., 2011) and their formation is thus consistent with elevated cortical tension following ADF/cofilin depletion. Cell defects were more severe following depletion of both ADF and cofilin relative to that of each isoform. The defects were efficiently rescued by expression of a single ADF/cofilin isoform suggesting that both isoforms act redundantly to control cytoskeletal organization, a conclusion also supported by previous studies (Hotulainen et al., 2005). Our data however, indicates the need for precise cumulative ADF/cofilin levels for achievement of distinct cellular functions.

We propose that ADF/cofilins regulate actin cytoskeleton dynamics in at least two significant ways (see model, Fig. 7M). In addition to F-actin severing and/or depolymerization we offer that ADF/cofilins regulate myosin II activity and actomyosin assembly by controlling access of myosins to F-actin. Our findings demonstrate that cofilin blocks myosin II binding to F-actin through direct competitive inhibition. Cofilin and myosin II are both known to induce allosteric effects on F-actin structure (Hild et al., 2010); this property in addition to steric hindrance may contribute to the manner in which each protein affects the other's ability to bind F-actin. Likewise, feedback mechanisms involving actin filament tension are likely to influence the activity of both cofilin and myosin II (Pavlov et al., 2007; Fernandez-Gonzalez et al., 2009; Hayakawa et al., 2011). Nevertheless, our biochemical studies support the sufficiency of a direct competitive binding model for cofilin regulation of myosin II activity. Reported affinities of myosin S1 for F-actin in the absence of ATP (rigor binding, K_d values ranging from 5 nM to 0.3 μM; Margossian and Lowey, 1978; Blanchoin et al., 1996) are generally greater than those reported for ADF/

cofilin ($K_d \approx 0.1$ μM; Andrianantoandro and Pollard, 2006). Our results suggest that the affinity of myosin S1 for F-actin, in the absence of ATP, relative to that of cofilin is not vastly dissimilar. At cellular ATP levels the affinity of myosin II for F-actin is reduced significantly ($K_d > 25$ μM; Prochniewicz et al., 2004) implying a substantive competitive advantage to ADF/cofilins in cells. Additionally, in contrast to myosin II, cells maintain relatively high levels of total ADF/cofilin proteins (for example, ~ 20 μM cofilin vs. ~ 1 μM myosin II in unicellular Acanthameoba; Pollard, 1982; Pollard et al., 2000). In fact, the relative concentrations at which we observe efficient competitive inhibition of myosin II by ADF/cofilin in our biochemical assays are comparable to those observed in cells. The precise activity of ADF/cofilins utilized in cells, however, will likely be dictated by local concentrations of the active proteins. ADF/cofilins sever F-actin at low binding densities but stabilize filaments at higher densities (Dedova et al., 2004; Andrianantoandro and Pollard, 2006), at which inhibition of myosin II binding is also expected.

Depletion of both ADF and cofilin triggered intense abnormal F-actin accumulation in cells. Following perturbations to ADF/cofilin this phenotype has been commonly interpreted as an indication of increased F-actin stabilization due to loss of depolymerization and/or severing activity. Remarkably however, our data indicate that abnormal cortical F-actin accumulation following ADF/cofilin depletion was primarily due to increased myosin II-dependent actin assembly. Abnormal actin structures which accumulated in ADF/cofilin-depleted cells disassembled within minutes following inhibition of myosin II activity with blebbistatin. This result strongly argues against impaired actin depolymerization as the primary defect responsible for the aberrant F-actin accumulation observed. In addition to its motor activity, myosin II bipolar filaments can cross-link actin filaments; and recent reports indicate this cross-linking activity is important (Vicente-Manzanares et al., 2007), as also suggested by our results. Earliest studies of ADF/cofilin function reported that along with actin depolymerization activity, these proteins also altered myosin II activity (Nishida et al., 1984; Abe and Obinata, 1989). Since then, the physiological significance of ADF/cofilin regulation of myosin had likely remained obscured due to the fact that actin defects resulting from excessive myosin II activity, following ADF/cofilin inhibition, are similar in many ways to those anticipated as a result of F-actin stabilization. Our results signify that it will be necessary to reevaluate many previous model systems of ADF/cofilin cellular function to properly discern between effects mediated by depolymerization and/or severing versus control of actomyosin assembly. The global requirement for these ADF/cofilin activities likely will not be mutually exclusive, however, our data indicate that they are markedly distinct.

As clearly evident by bleb phenotypes following their depletion, our findings suggest that ADF/cofilin proteins are crucial for restricting myosin II activity in maintaining normal homeostatic actomyosin cytoarchitecture and cortical tension. This function for ADF/cofilin is of particular importance during mitotic cell division where loss of ADF/cofilin activity results in abnormal metaphase blebbing, larger polar membrane blebs at cytokinesis and detrimental karyokinesis defects. Our data are in agreement with those from theoretical modeling suggesting the necessity of tight control of cortical tension during cytokinesis (Sedzinski et al., 2011). Our findings are consistent with roles for ADF/cofilin in the regulation of both karyokinesis and cytokinesis, indicating that deregulated ADF/cofilin activity may contribute to aneuploidy by several means. The multiple requirements for ADF/cofilin in cell division advocates caution in deriving conclusions about the cause of multinucleation phenotypes following ADF/cofilin perturbations.

Actomyosin contractility and cytoskeletal tension impinge on many cell functions and when deregulated may contribute to pathological conditions such as cancer. Indeed, it was recently reported that a Rho kinase pathway involving the cofilin kinase, LIMK, drives epidermal

tumor growth through control of actomyosin contractility (Samuel et al., 2011). The precise manner by which LIMK contributed to actomyosin contractility was not examined. Here, we define a mechanism by which LIMK, through cofilin phospho-inactivation, can directly promote increased actomyosin contractility and intracellular tension (see model Fig. 7M). Migration of tumor cells in certain environments appears dependent upon actomyosin mediated membrane blebs. Results herein indicate an important role for ADF/cofilin in control of normal bleb dynamics, signifying other ways in which the cofilin pathway may be utilized in pathology. Thus, our findings identify a new framework in which to examine ADF/cofilin function in numerous aspects of both normal development and pathogenesis.

Experimental Procedures

Procedures for live cell imaging, siRNA descriptions and cosedimentation assays are detailed in the Supplemental Experimental Procedures.

Cell culture and reagents

HeLa (Kyoto strain) cells, were grown in DMEM supplemented with 10% fetal bovine serum (Atlas Biologicals). Antibodies were rabbit, myosin IIA, myosin IIB, myosin IIC, p-myosin light chain (Ser19), (Cell Signaling); myosin IIB (blots), mouse anti-α-tubulin, anti-actin (Sigma); GAPDH (Millipore); cofilin (Cytoskeleton). Antibodies to cofilin/ADF (1439) have been described (Shaw et al., 2004).

Transfections

Cells were transfected with 40–50 nM of siRNAs at the time of plating and again 24 h later with either Lipofecatamine RNAiMax or Lipofectamine 2000 (Invitrogen) using manufacturer's protocols. Cell lysates and western blots were done as described (Wiggan et al., 2006).

Immunofluorescence Staining and Microscopy

Cells grown on glass coverslips were fixed and stained as described (Wiggan et al., 2006). Fluorescent images were acquired with an Olympus IX81 spinning disk confocal (CSU22 head) microscope with either 100x/1.40 NA, 60x/1.42 NA or 40x/1.35 NA objectives. Images were acquired with a Photometrics Cascade II CCD camera using SlideBook (Intelligent Imaging Innovations) software and processed with Metamorph and/or Adobe Photoshop software. The Student's t-test was used for statistical analysis of P values.

Proteins

Rabbit skeletal muscle actin was prepared by the methods of Pardee and Spudich (Pardee and Spudich, 1982) and as detailed (Chen et al., 2004). Rabbit skeletal muscle myosin preparation and generation of subfragment-1 (S1) by chymotryptic digestion were as detailed (Margossian and Lowey, 1982). Purified recombinant ADF/cofilin proteins were obtained as described (Chen et al., 2004).

Supplementary Material

Refer to Web version on PubMed Central for supplementary material.

Acknowledgments

We thank Imarhia Enogieru for assistance in making reagents and the BMB Cytoskeletal group for helpful comments on this work. Supported in part by NIH grants NS064217 (OW), NS43115, NS40371 (JRB), and a grant from the Pew Biomedical Scholars Program (JGD).

References

Abe H, Obinata T. An actin-depolymerizing protein in embryonic chicken skeletal muscle: purification and characterization. J Biochem. 1989; 106:172–180. [PubMed: 2777748]

Andrianantoandro E, Pollard TD. Mechanism of actin filament turnover by severing and nucleation at different concentrations of ADF/cofilin. Mol Cell. 2006; 24:13–23. [PubMed: 17018289]

Bamburg JR, Bernstein BW. Roles of ADF/cofilin in actin polymerization and beyond. F1000 Biol Rep. 2010; 19(2):62. [PubMed: 21173851]

Blanchoin L, Didry D, Carlier MF, Pantaloni D. Kinetics of association of myosin subfragment-1 to unlabeled and pyrenyl-labeled actin. J Biol Chem. 1996; 271:12380–12386. [PubMed: 8647841]

Bray D, White JG. Cortical flow in animal cells. Science. 1988; 19(239):883–888. [PubMed: 3277283]

Charras G, Paluch E. Blebs lead the way: how to migrate without lamellipodia. Nat Rev Mol Cell Biol. 2008; 9:730–736. [PubMed: 18628785]

Chen H, Bernstein BW, Sneider JM, Boyle JA, Minamide LS, Bamburg JR. In vitro activity differences between proteins of the ADF/cofilin family define two distinct subgroups. Biochemistry. 2004; 43:7127–7142. [PubMed: 15170350]

Clark K, Langeslag M, Figdor CG, van Leeuwen FN. Myosin II and mechanotransduction: a balancing act. Trends Cell Biol. 2007; 17:178–186. [PubMed: 17320396]

Dedova IV, Nikolaeva OP, Mikhailova VV, dos Remedios CG, Levitsky DI. Two opposite effects of cofilin on the thermal unfolding of F-actin: a differential scanning calorimetric study. Biophys Chem. 2004; 110:119–128. [PubMed: 15223149]

DesMarais V, Ghosh M, Eddy R, Condeelis J. Cofilin takes the lead. J Cell Sci. 2005; 118:19–26. [PubMed: 15615780]

Fernandez-Gonzalez R, Simoes Sde M, Roper JC, Eaton S, Zallen JA. Myosin II dynamics are regulated by tension in intercalating cells. Developmental Cell. 2009; 17:736–743. [PubMed: 19879198]

Gunsalus KC, Bonaccorsi S, Williams E, Verni F, Gatti M, Goldberg ML. Mutations in twinstar, a Drosophila gene encoding a cofilin/ADF homologue, result in defects in centrosome migration and cytokinesis. J Cell Biol. 1995; 131:1243–1259. [PubMed: 8522587]

Hayakawa K, Tatsumi H, Sokabe M. Actin filaments function as a tension sensor by tension-dependent binding of cofilin to the filament. J Cell Biol. 2011; 195:721–727. [PubMed: 22123860]

Hild G, Bugyi B, Nyitrai M. Conformational dynamics of actin: effectors and implications for biological function. Cytoskeleton (Hoboken, NJ). 2010; 67:609–629.

Hotulainen P, Paunola E, Vartiainen MK, Lappalainen P. Actin-depolymerizing factor and cofilin-1 play overlapping roles in promoting rapid F-actin depolymerization in mammalian nonmuscle cells. Mol Biol Cell. 2005; 16:649–664. [PubMed: 15548599]

Kolega J, Janson LW, Taylor DL. The role of solation-contraction coupling in regulating stress fiber dynamics in nonmuscle cells. J Cell Biol. 1991; 114:993–1003. [PubMed: 1874793]

Kovacs M, Toth J, Hetenyi C, Malnasi-Csizmadia A, Sellers JR. Mechanism of blebbistatin inhibition of myosin II. J Biol Chem. 2004; 279:35557–35563. [PubMed: 15205456]

Kumar S, Maxwell IZ, Heisterkamp A, Polte TR, Lele TP, Salanga M, Mazur E, Ingber DE. Viscoelastic retraction of single living stress fibers and its impact on cell shape, cytoskeletal organization, and extracellular matrix mechanics. Biophys J. 2006; 90:3762–3773. [PubMed: 16500961]

Lecuit T, Lenne PF, Munro E. Force Generation, Transmission, and Integration During Cell and Tissue Morphogenesis. Annu Rev Cell Dev Biol. 201010.1146/annurev-cellbio-100109-104027

Lorenz M, Holmes KC. The actin-myosin interface. Proc Natl Acad Sci U S A. 2010; 107:12529–12534. [PubMed: 20616041]

Mannherz HG, Ballweber E, Galla M, Villard S, Granier C, Steegborn C, Schmidtmann A, Jaquet K, Pope B, Weeds AG. Mapping the ADF/cofilin binding site on monomeric actin by competitive cross-linking and peptide array: evidence for a second binding site on monomeric actin. J Mol Biol. 2007; 366:745–755. [PubMed: 17196218]

Margossian SS, Lowey S. Interaction of myosin subfragments with F-actin. Biochemistry. 1978; 17:5431–5439. [PubMed: 153150]

Margossian SS, Lowey S. Preparation of myosin and its subfragments from rabbit skeletal muscle. Methods Enzymol. 1982; 85(Pt B):55–71. [PubMed: 6214692]

McGough A. F-actin-binding proteins. Curr Opin Struct Biol. 1998; 8:166–176. [PubMed: 9631289]

Nishida E, Maekawa S, Sakai H. Cofilin, a protein in porcine brain that binds to actin filaments and inhibits their interactions with myosin and tropomyosin. Biochemistry. 1984; 23:5307–5313. [PubMed: 6509022]

Paavilainen VO, Oksanen E, Goldman A, Lappalainen P. Structure of the actin-depolymerizing factor homology domain in complex with actin. J Cell Biol. 2008; 182:51–59. [PubMed: 18625842]

Paluch E, Sykes C, Prost J, Bornens M. Dynamic modes of the cortical actomyosin gel during cell locomotion and division. Trends Cell Biol. 2006; 16:5–10. [PubMed: 16325405]

Pardee JD, Spudich JA. Purification of muscle actin. Methods Enzymol. 1982; 85(Pt B):164–81. [PubMed: 7121269]

Pavlov D, Muhlrad A, Cooper J, Wear M, Reisler E. Actin filament severing by cofilin. J Mol Biol. 2007; 365:1350–1358. [PubMed: 17134718]

Pollard TD. Structure and polymerization of Acanthamoeba myosin-II filaments. J Cell Biol. 1982; 95:816–825. [PubMed: 7153247]

Pollard TD, Blanchoin L, Mullins RD. Molecular mechanisms controlling actin filament dynamics in nonmuscle cells. Annu Rev Biophys Biomol Struct. 2000; 29:545–576. [PubMed: 10940259]

Pollard TD, Borisy GG. Cellular motility driven by assembly and disassembly of actin filaments. Cell. 2003; 112:453–465. [PubMed: 12600310]

Prochniewicz E, Walseth TF, Thomas DD. Structural dynamics of actin during active interaction with myosin: different effects of weakly and strongly bound myosin heads. Biochemistry. 2004; 43:10642–10652. [PubMed: 15311925]

Rankin KE, Wordeman L. Long astral microtubules uncouple mitotic spindles from the cytokinetic furrow. J Cell Biol. 2010; 190:35–43. [PubMed: 20603328]

Samuel MS, Lopez JI, McGhee EJ, Croft DR, Strachan D, Timpson P, Munro J, Schroder E, Zhou J, Brunton VG, Barker N, Clevers H, Sansom OJ, Anderson KI, Weaver VM, Olson MF. Actomyosin-mediated cellular tension drives increased tissue stiffness and beta-catenin activation to induce epidermal hyperplasia and tumor growth. Cancer Cell. 2011; 19:776–791. [PubMed: 21665151]

Sedzinski J, Biro M, Oswald A, Tinevez JY, Salbreux G, Paluch E. Polar actomyosin contractility destabilizes the position of the cytokinetic furrow. Nature. 2011; 476:462–466. [PubMed: 21822289]

Shaw AE, Minamide LS, Bill CL, Funk JD, Maiti S, Bamburg JR. Cross-reactivity of antibodies to actin- depolymerizing factor/cofilin family proteins and identification of the major epitope recognized by a mammalian actin-depolymerizing factor/cofilin antibody. Electrophoresis. 2004; 25:2611–2620. [PubMed: 15300782]

Straight AF, Cheung A, Limouze J, Chen I, Westwood NJ, Sellers JR, Mitchison TJ. Dissecting temporal and spatial control of cytokinesis with a myosin II Inhibitor. Science. 2003; 299:1743–1747. [PubMed: 12637748]

Tinevez JY, Schulze U, Salbreux G, Roensch J, Joanny JF, Paluch E. Role of cortical tension in bleb growth. Proc Natl Acad Sci U S A. 2009; 106:18581–18586. [PubMed: 19846787]

Van Troys M, Huyck L, Leyman S, Dhaese S, Vandekerkhove J, Ampe C. Ins and outs of ADF/cofilin activity and regulation. Eur J Cell Biol. 2008; 87:649–667. [PubMed: 18499298]

Vicente-Manzanares M, Ma X, Adelstein RS, Horwitz AR. Non-muscle myosin II takes centre stage in cell adhesion and migration. Nat Rev Mol Cell Biol. 2009; 10:778–790. [PubMed: 19851336]

Vicente-Manzanares M, Zareno J, Whitmore L, Choi CK, Horwitz AF. Regulation of protrusion, adhesion dynamics, and polarity by myosins IIA and IIB in migrating cells. J Cell Biol. 2007; 176:573–580. [PubMed: 17312025]

Wiggan O, Shaw AE, Bamburg JR. Essential requirement for Rho family GTPase signaling in Pax3 induced mesenchymal-epithelial transition. Cell Signal. 2006; 18:1501–1514. [PubMed: 16442263]

Highlights

- Cofilin regulates myosin II function through competitive binding to F-actin
- Cofilin modulates actin filament tension and contractility
- Cofilin controls normal cortical stability, membrane dynamics and karyokinesis
- Excessive myosin activity drives major cellular defects following cofilin depletion

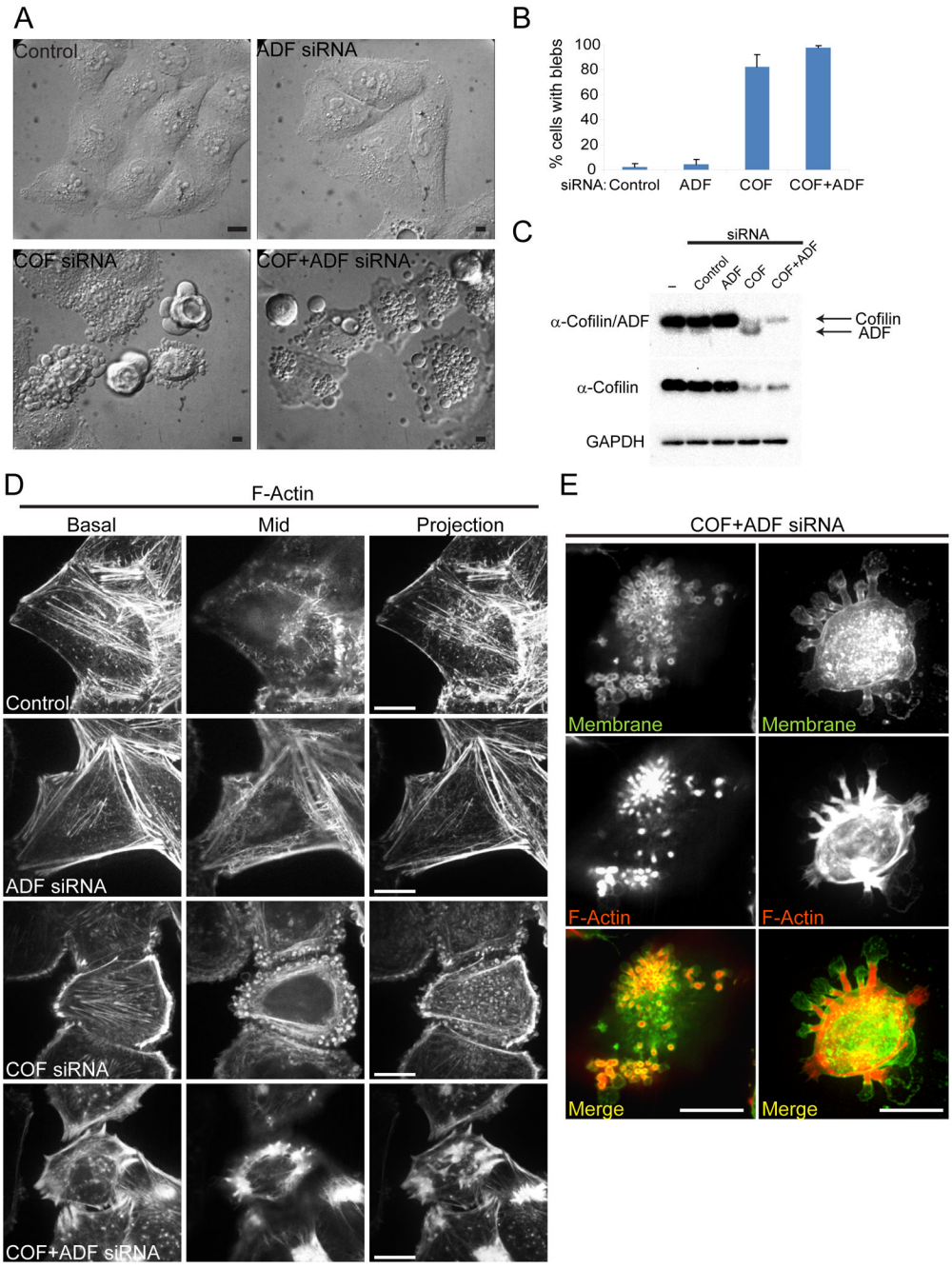

Figure 1. ADF/cofilin silencing results in distinct cell morphological defects

HeLa cells treated with indicated siRNAs were examined at 72h post treatment. (A) DIC images of live cells. (B) Quantification of cells with plasma membrane blebs. Values are mean ± sd, n > 200 cells/treatment from at least 3 experiments. (C) Representative blots of total ADF/cofilin, cofilin (cofilin specific antibody), and GAPDH (loading control) following siRNA treatment. (D) Representative confocal sections (apical, mid) and maximum intensity projections of F-actin fluorescence staining. (E) Apical confocal sections depicting abnormal F-actin accumulation at the base of rosettes of small membrane blebs (left panels) and z-projections showing similar F-actin accumulation at the base of large membrane protrusions (right panels) in fixed ADF/cofilin depleted cells. Bars, 10 μm.

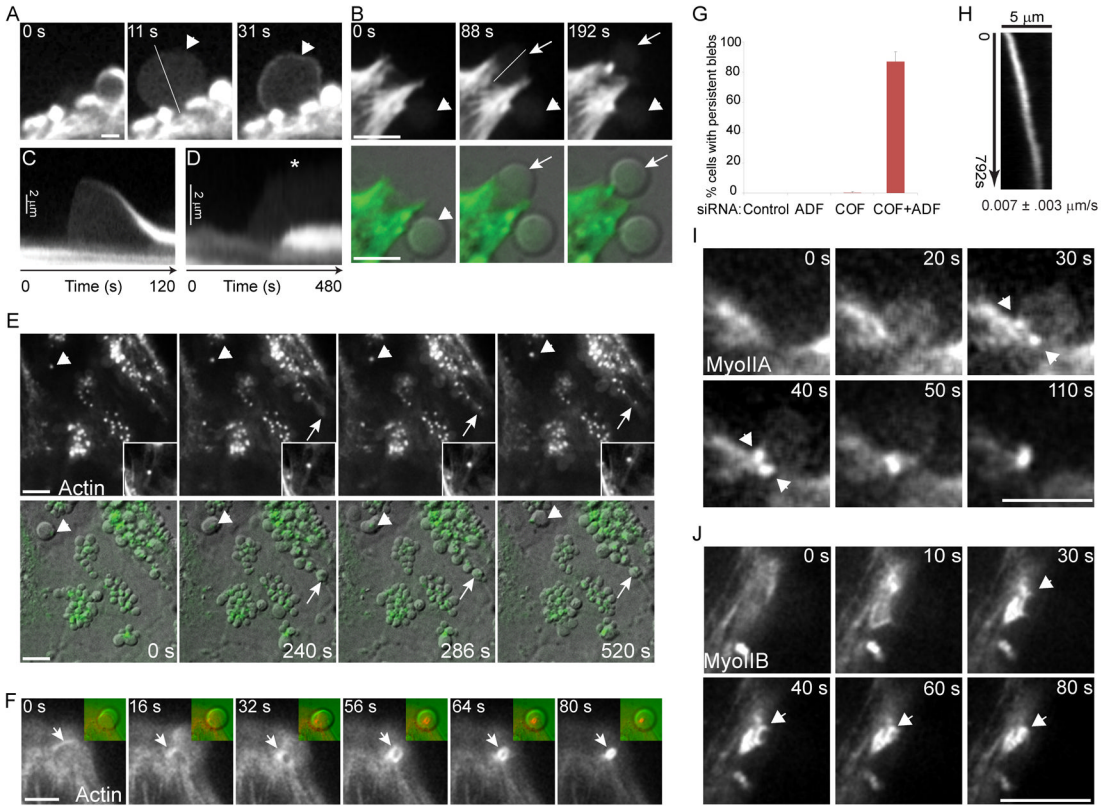

Figure 2. Formation of persistent blebs and aberrant contractile actomyosin structures in cells depleted of ADF and cofilin

(A) Representative time series showing recruitment of actin to the cortex of a dynamic bleb (arrowhead). (B) Persistent blebs fail to assemble a new actin cortex (arrowhead, GFP-actin upper panels; DIC overlay, lower panels). Arrow shows emergence of a new persistent bleb. Bars, 5 μm (A, B). (C) Kymograph of the bleb in (A, arrowhead) along line shown (A; t = 11s). (D) Kymograph of bleb activity for the bleb in (B, arrow) along line shown (B; t= 88s). (E) Time-lapse series of GFP-actin (upper panels; green, bottom panels) overlaid to DIC images (bottom panels) in HeLa cells depleted of both ADF and cofilin shows accumulation of actin at blebs which fail to retract. Actin accumulates at blebs after their initiation (arrow). Insets show magnified images of an actin aggregate associated with a bleb (arrowhead) which migrates along actin filaments towards the cell body (top of image). Bar 10 μm. (F) Time series of GFP-actin shows formation of a contractile actin ring structure (arrow) at the base of a bleb (see Movie S1). Insets show the same field for actin (pseudocolored red) overlain to a DIC image of the bleb (pseudocolored green). (G) Quantification of persistent bleb formation. Values are mean ± sd, n > 200 cells/treatment from at least 3 experiments. (H) Kymograph showing motility of the bleb actin aggregate depicted in (E, insets). Mean velocity ± sd, n=9. (I and J) Accumulation of GFP-MyoIIA (I, arrowheads) and GFP-MyoIIB (J, arrowheads) at contractile structures at the base of blebs in COF+ADF depleted cells. Bars, 5 μm.

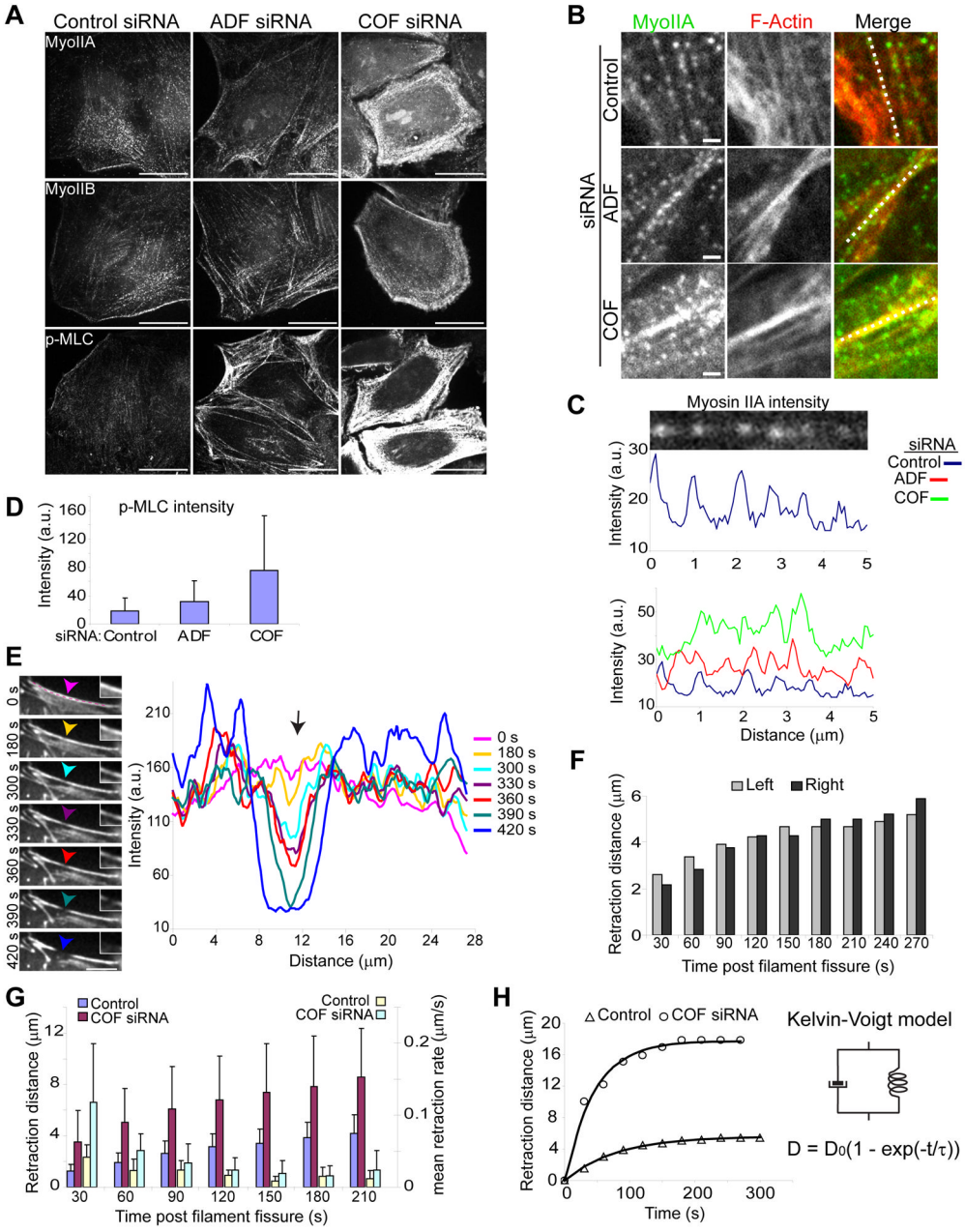

Figure 3. Increased actomyosin assembly and cortical contractility in ADF/cofilin depleted cells

(A) Representative confocal immunofluorescence images show elevated cortical myosin II recruitment following cofilin siRNA treatment. Bars, 10 μm.

(B and C) Intensity linescans (B, white lines in merged images) of myosin foci, detected as distinct peaks in plots (illustrated in C, upper panels) along actin filaments plotted in (C). Bars, 1 μm. (D) Quantification of p-MLC intensity at cortical cell regions. Values are mean ± sd, n ≥18 cells/treatment. (E) Illustrative time series of F-actin fluorescence intensity (RFP-Lifeact) along a contractile cortical F-actin bundle (line in image, t = 0s) graphed (right) over time following treatment of control cells with latrunculin B. Arrows in images and graph depict the position at which fiber fissure occurs (t = 390s), magnified in insets. Note the decrease in actin intensity coupled to increased intensity on both sides of the point of fissure, pre- and post-breakage. Bar, 10 μm. (F) Retraction kinetics of fiber segments to

the left and right of the point of fissure for the fiber depicted in (E). (G) Retraction kinetics of cortical fibers with spontaneous breakage following latrunculin B treatment of control and cofilin depleted cells. Values are mean ± sd, n= 13 control; n = 12 COF siRNA. (H) Graph of fiber retraction kinetics following fissure in a control or COF siRNA treated cell. Solid lines represent a fit to the Kelvin-Voigt viscoelastic model, represented by a viscous dashpot in parallel with an elastic spring. D is the measured retraction distance at time, t, D_0 is the derived asymptotic retraction distance and the derived time constant, τ, is the ratio of viscosity to the elastic modulus.

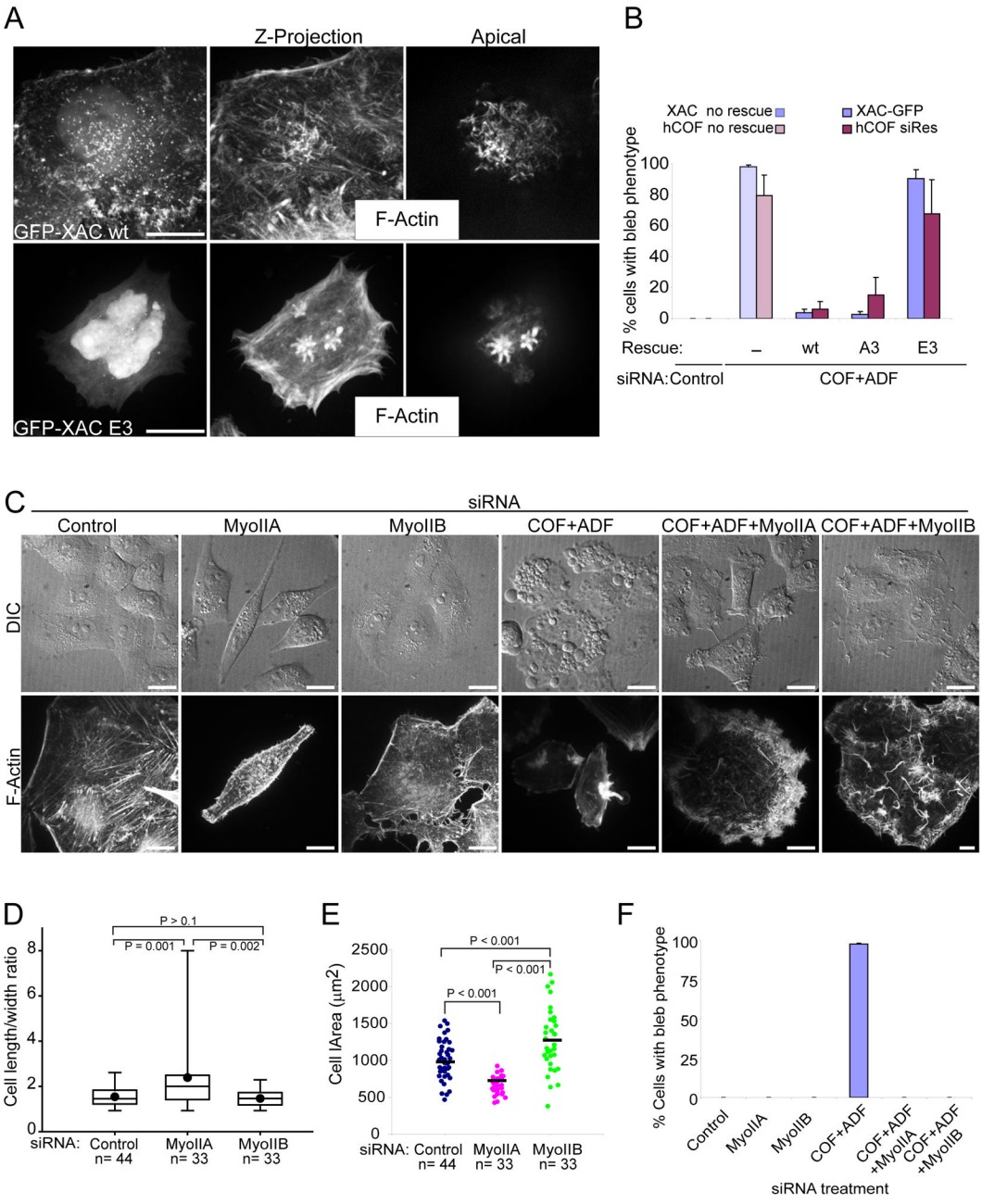

Figure 4. Rescue of cytoskeletal and bleb defects in COF+ADF depleted cells by ectopic ADF/cofilin expression or myosin II silencing

(A) Confocal fluorescence images of cells depleted of both ADF and cofilin and ectopically expressing either wild type Xenopus ADF/cofilin (GFP-XAC wt) or a constitutively inactive cofilin (GFP-XAC E3). (B) Quantification of the rescue of bleb phenotypes by adenoviral mediated XAC or transfected hCOF siRNA resistant plasmid expression. Values are mean ± sd, n > 400 from at least 3 experiments. (C) Effects of co-depletion of myosin II isoforms and ADF/cofilin on cell morphology (live cell DIC images, upper panels) and F-actin organization (fluorescence images, lower panels). (D) Cells are more elongated following myoIIA silencing. Box lines are 25%, median and 75%, dots are mean values and whiskers show full data range. (E) Increased cell area following myoIIB silencing. Bars are mean

values. (F) Quantification of bleb phenotypes following co-depletion of ADF/cofilin and myosin II. Values are mean ± sd, n ≥ 700 cells/treatment from at least 3 experiments. Bars, 10 μm (A, C).

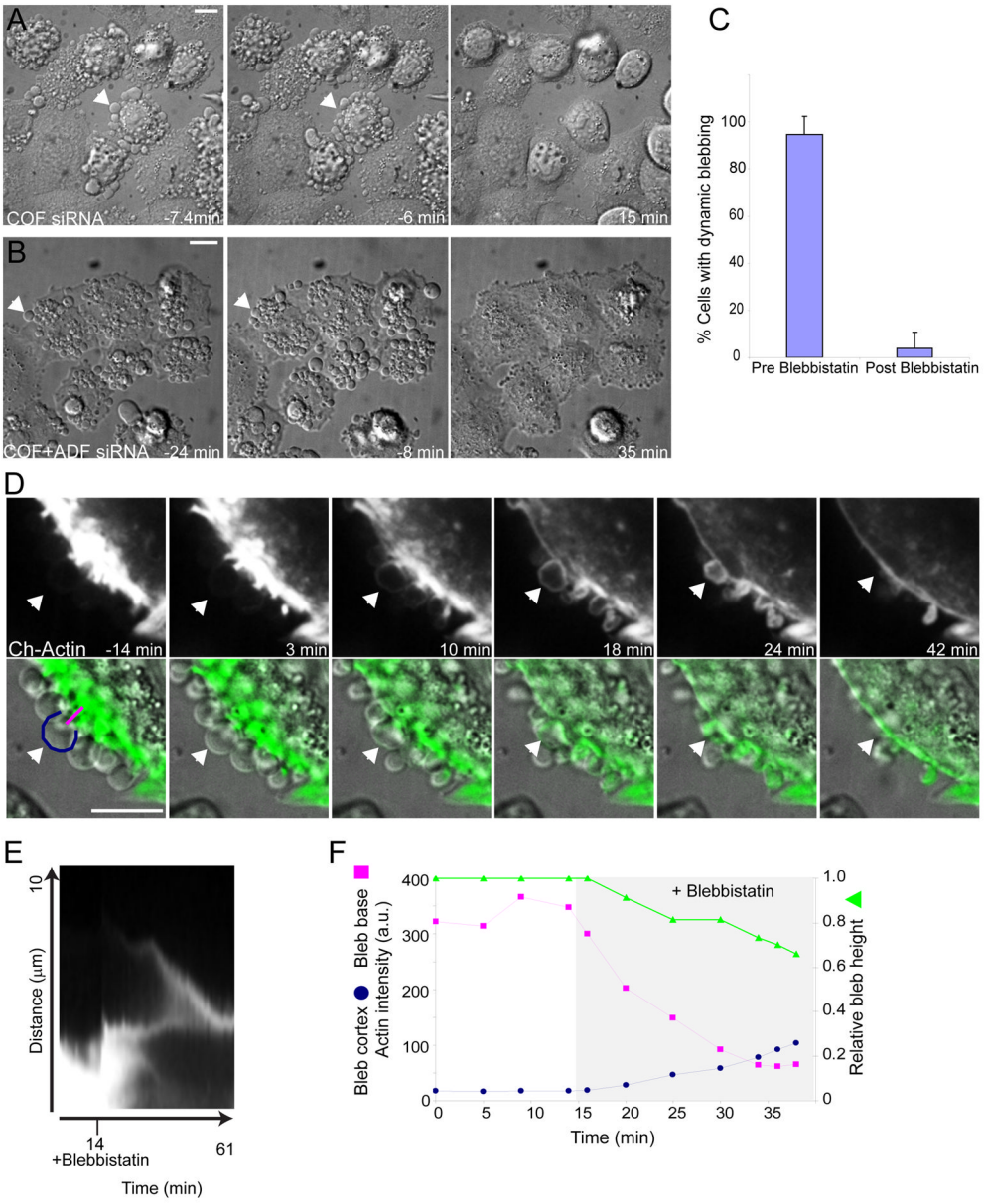

Figure 5. Blebbing and abnormal cortical actin accumulation in ADF/cofilin depleted cells is dependent upon myosin II activity

(A and B) DIC time-lapse series showing inhibition of dynamic blebbing (A, arrowhead) in cofilin depleted cells and retraction of persistent blebs (B, arrowhead) in cells depleted of both ADF and cofilin, following blebbistatin treatment. Time is relative to blebbistatin addition. See also Movie S2. (C) Quantification of blebbing prior to and after blebbistatin treatment of cofilin and ADF+COF depleted cells. Values are mean ± sd, n = 123, from 3 experiments. (D) Confocal time-lapse series of mCherry-actin (upper panels; and pseudocolored green in DIC overlays, lower panels; see also Movie S3) in ADF/cofilin depleted cells pre and post drug treatment. Arrowhead depicts a persistent bleb which retracts following blebbistatin addition. (E) Kymograph of bleb depicted by arrowhead (D). (F) Graph of actin intensities along lines shown in (D, t = −14m, bottom panel) during retraction of the depicted bleb. Bars, 10 μm.

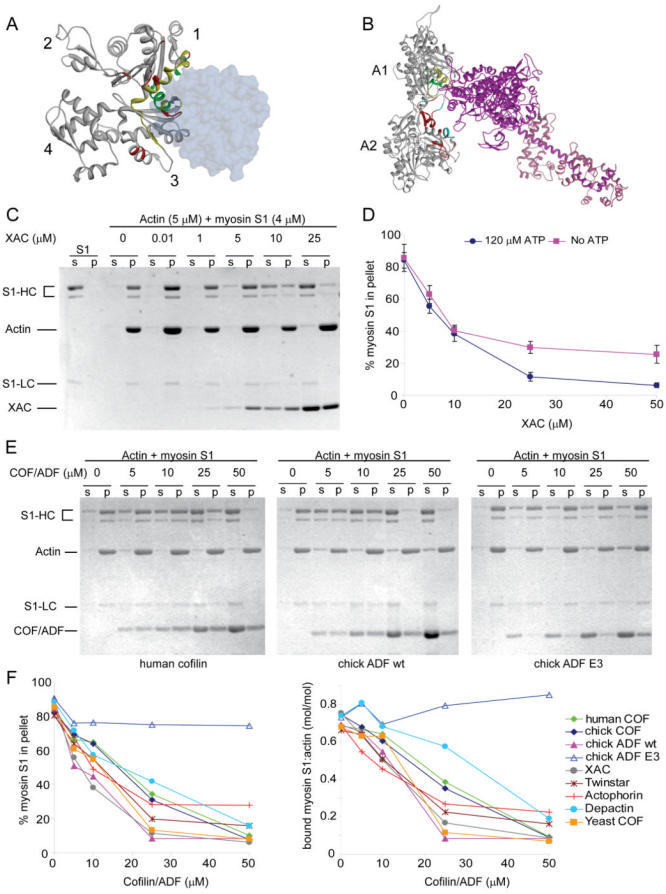

Figure 6. ADF/cofilin inhibits myosin S1 binding to F-actin

(A) Structure of the ADF-homology domain (ADF-H, blue) bound to G-actin (ribbon structure) (Paavilainen et al., 2008). ADF-H binds to a hydrophobic pocket between subdomains 1 and 3 of actin. Putative sites of interaction on actin for ADF/cofilin are colored green, those for myosin S1 are in red, and overlapping sites yellow. (B) Model structure of myosin S1 (heavy chain, violet; light chain, pink) interaction with F-actin (2 monomers, grey) (Lorenz and Holmes, 2010). Putative positions of interaction at the primary actin binding site (monomer A1) for ADF/cofilin are green and secondary sites of interaction (monomer A2), red. Overlapping sites for ADF/cofilin and myosin S1 are yellow (monomer A1) and cyan (monomer A2). (C) Coomassie-Blue stained gels of supernatants (s) and pellets (p) from a cosedimentation assay where myosin subfragment-1 (S1) was preincubated with F-actin in the presence of 120 μM ATP prior to addition of Xenopus cofilin (XAC), as indicated. S1-HC, myosin S1 heavy chain, lower band corresponds to a common ~ 76 kDa proteolytic product; S1-LC, myosin light chain A1. (D) Quantification of actin bound myosin S1 following simultaneous exposure of both myosin S1 and XAC to F-actin in the presence or absence of ATP. Results are mean of 3 experiments ± sd. (E and F) Representative gels (E) and quantification (F) of actin bound myosin S1 in the presence of ADF/cofilins from human, chick, xenopus, drosophila (twinstar), acanthamoeba (actophorin), starfish (depactin) and yeast. Graphs are mean of 3 experiments.

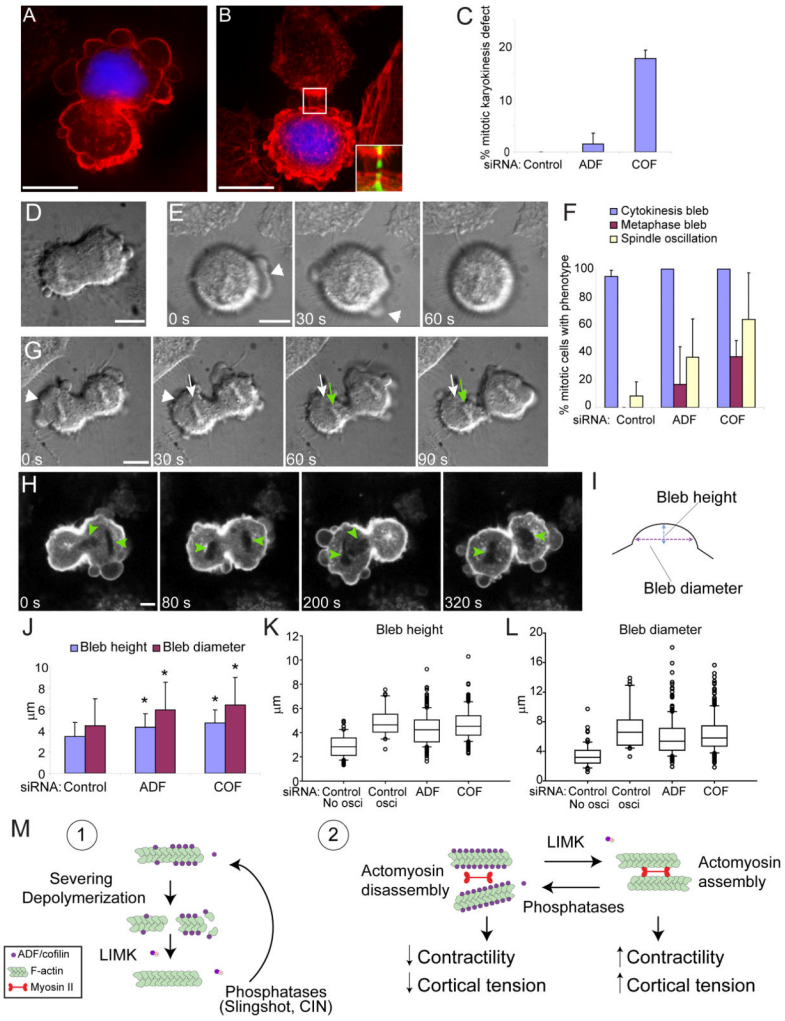

Figure 7. ADF/cofilin depletion results in mitotic karyokinesis defects

(A and B) Fluorescence images of cofilin depleted cells at telophase (A) and late cytokinesis (B), labeled for F-actin (red) and DNA (blue). Boxed region in (B) is expanded in inset and shows F-actin (red)/microtubule (green) overlay. (C) Quantification of karyokinesis defects. Values are mean ± sd, n > 170 from 3 experiments. (D and E) DIC images of blebbing at cytokinesis in control cells (D; see Movie S4) and of dynamic blebbing (E, arrowhead in time series) during metaphase in ADF depleted cells. (F) Quantification of cytokinetic bleb and spindle displacement phenotypes. Values are mean ± sd, n ≥ 24 from at least 3 experiments. (G and H) Time-lapse series showing weak spindle displacement behavior (G, DIC images of ADF depleted cells) and strong spindle oscillation behavior (H, GFP-GPI fluorescence images of cofilin depleted cells; see also Movie S5). Arrowhead in (G) shows retraction of a large bleb, white and green arrows show the initial and displaced chromosome positions respectively. Arrowheads in (H) mark chromosome positions. Scale bar for all images, 10µm. (I–L) Bleb height and diameter measurements during cytokinesis. (J) Values are mean ± sd (Control n=18 cells, 110 blebs; ADF n=22 cells, 241 blebs; COF n= 14 cells, 197 blebs). *, P < 0.001 relative to control, t-test. Box lines are 25%, median and 75%, whiskers show 10–90% range and circles are outliers (K, L). (M) Model depicting two physiologically significant functions for ADF/cofilin: 1) F-actin turnover through filament severing and/or depolymeriztion, 2) Actomyosin assembly through inhibition of myosin II binding to F-actin.